Chapter 4
Design for Body Bending

In this chapter we consider the overall body structure supported and loaded similar to a single beam. The supporting points and loads are applied symmetrically to the vehicle center line; that is, loads on the right side are the same as loads on the left side. We will consider two types of body bending requirements: strength and stiffness.

4.1 Body Bending Strength Requirement

A most basic structure requirement is to locate and retain the vehicle subsystems in the correct positions. Powertrain, occupants, suspension, etc. must be supported by the body structure. Consider a vehicle at rest with the weight of the vehicle subsystems being supported by the body structure, which we will idealize as a beam in the side view, Figure 4.1. A requirement for this structure is that it does not fail under this loading condition.

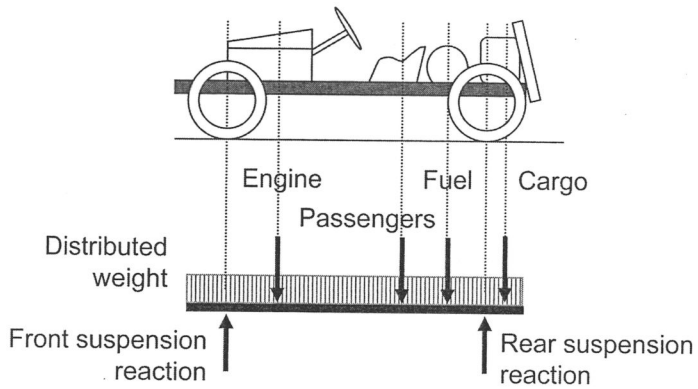

Figure 4.1 Body loaded by subsystem weight.

Let us look at the bending moments being applied to the structure under this condition. Using standard bending moment analysis techniques, we can identify the shear loads and moments being applied at any position along the length of the structure, Figure 4.2 [1]. A strength requirement for this body structure is to react these moments without failure.

More severe bending conditions than static weight loading can be imagined. The first is dynamic loading where the inertia loads of the subsystem exert larger forces during use than in the static condition. This condition can be addressed by multiplying the forces and moments of the static case by a dynamic acceleration factor. A typically used factor is 2-g loading—application of twice the static loads. A second condition is jacking or towing, where one support point is moved to an end of the vehicle, Figure 4.3. For this condition, we have taken an extreme case in which passenger loads are present. Although not typical, this represents a possible case for which the customer would not expect structural failure. Both front or rear jacking result in a larger maximum bending moment than that under static loading, as shown in Figure 4.4.

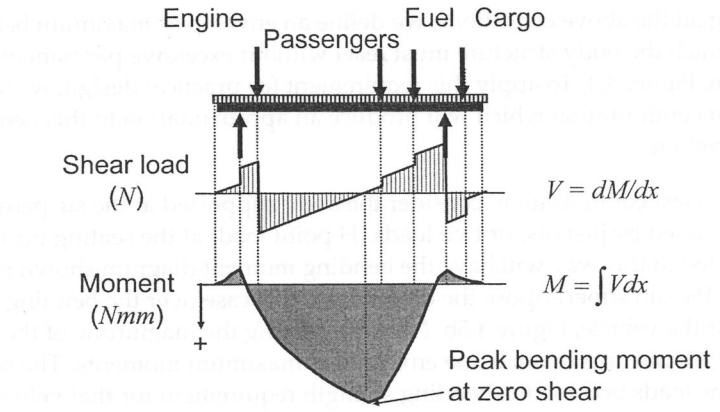

Figure 4.2 Shear and bending moment due to subsystem weight.

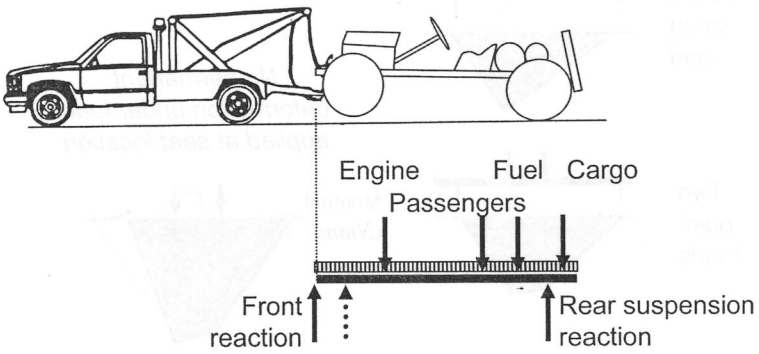

Figure 4.3 Front towing or jacking condition.

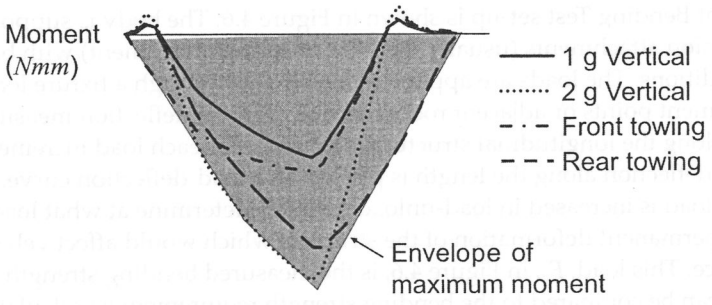

Figure 4.4 Envelope of moments.

Considering all the above conditions, we define an envelop of maximum bending moments which the body structure must react without excessive permanent deformation, Figure 4.4. To apply this requirement for practical design, we seek a simple test configuration which will produce an approximation to this bending moment envelope.

To define this test configuration, consider the body supported at the suspension points and loaded by just one or two loads (H point load) at the seating position. A beam loaded in this way will have the bending moment diagram shown in Figure 4.5a. We can superimpose the diagram for this case over the bending moments for the vehicle, Figure 4.5b. Now, by varying the magnitude of the H point loads, we can approximate the envelope of maximum moments. The resulting values for the loads become the bending strength requirement for that vehicle. This simpler condition is referred to as the H Point Bending Test because, in practice, the loads are applied at the seating location (H point).

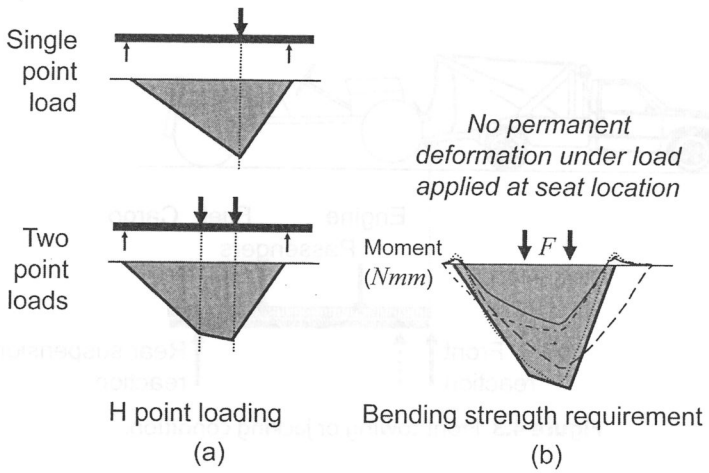

Figure 4.5 Equivalent load at passenger position.

The H Point Bending Test set-up is shown in Figure 4.6. The body is supported at the suspension attachments (usually the strut or spring attachment) with ball and socket conditions. The loads are applied in increments through a fixture loading the seat attachment points or adjacent rocker section. Vertical deflection measurements are taken along the longitudinal structural elements. For each load increment, the maximum deflection along the length is plotted on a load-deflection curve. The maximum load is increased in load-unload cycles to determine at what load there remains a permanent deformation of the structure which would affect vehicle performance. This load, F_s, in Figure 4.6, is the measured bending strength for the body, and can be compared to the bending strength requirement as calculated by the procedure shown in Figure 4.5b.

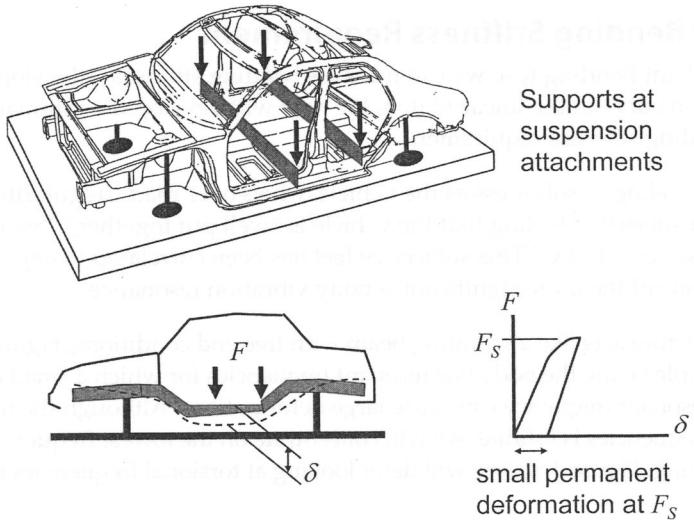

Figure 4.6 H point bending test convention.

Such a standardized bending test allows the comparison of competitive vehicles. Figure 4.7 shows the maximum bending moment for a sampling of 20 vehicles. Note that the body bending strength requirement depends on the bending moment analysis for the particular vehicle under consideration. Those bending moments depend on the placement of the subsystem mass, and the longitudinal dimensions of the vehicle, particularly the wheelbase.

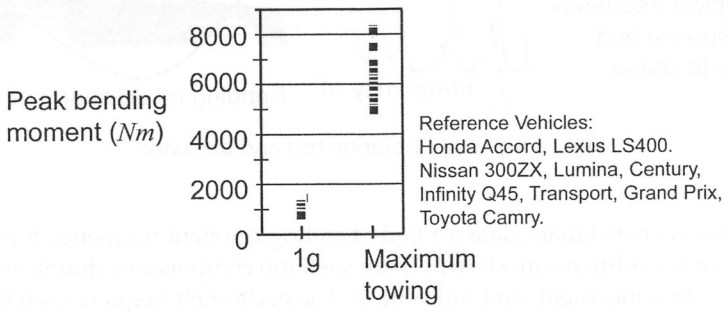

Figure 4.7 Bending test strength benchmarking. (Data courtesy of the American Iron and Steel Institute, UltraSteel Auto Body)

4.2 Body Bending Stiffness Requirement

From the H Point Bending test, we can measure bending stiffness—the slope of the load-deflection curve in the linear region. We now will develop the rationale for setting a bending stiffness requirement.

Consider the feeling of solidness as the vehicle drives over road irregularities. Solidness is a subjective feeling that the vehicle is "well put together," "vault-like," and not "loose" or "shaky." This subjective feel has been correlated to engineering parameters; one of the more significant is body vibration resonance.

The body structure acts like a vibrating beam with free end conditions, Figure 4.8a. As with a simple beam, the body has resonant frequencies for which a small dynamic force at the resonant frequency can cause large deformations. Although the number of resonant frequencies is infinite, we will concentrate on the lowest frequency of primary bending, Figure 4.8b (we will defer looking at torsional frequencies to a later chapter).

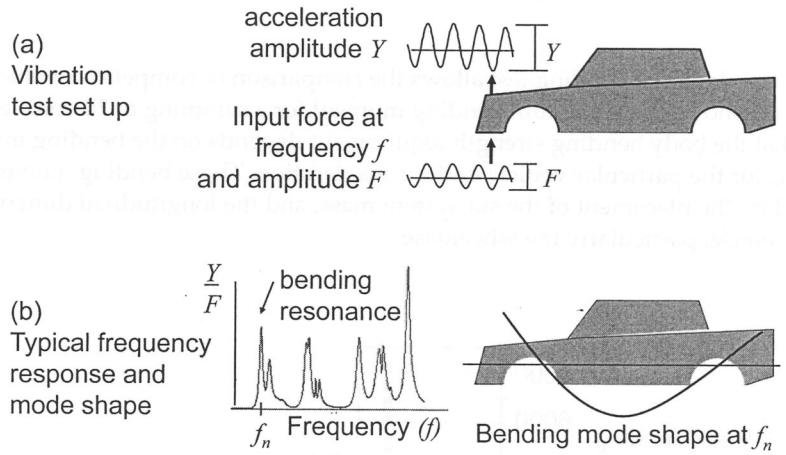

Figure 4.8 Body vibration test and behavior.

Figure 4.9 shows benchmark data for body bending resonant frequency for 47 vehicles. Three conditions are shown; Body shell (no components, doors, or glass), body shell with windshield, and full vehicle. The body shell frequencies with or without glass are similar, and are in general higher than the full vehicle condition. This is because the additional subsystem mass in the vehicle condition reduces the resonant frequency, as we will discuss below.

Customer testing in ride mules [2] where the bending resonant frequency could be varied, Figure 4.10, have shown that, to achieve the feeling of solidness, a desirable range for vehicle bending frequency is from 22–25 Hz. This frequency range is relatively free from major exciting forces and responders, and is also in a range in which humans are less sensitive to vibration.

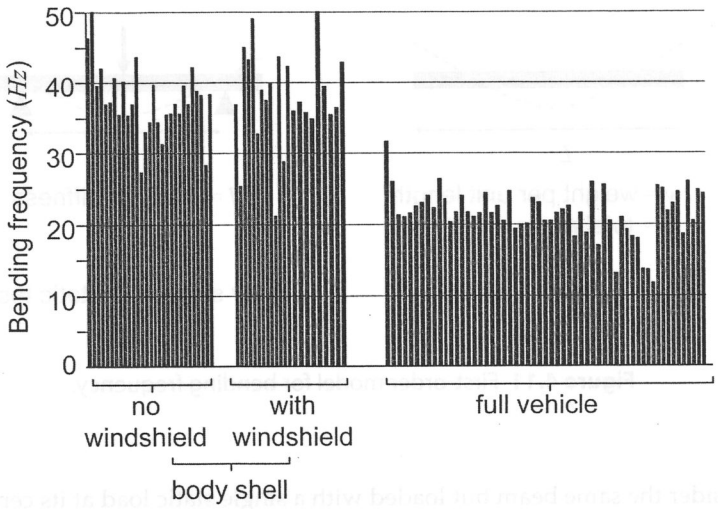

Figure 4.9 Bending resonant frequency benchmarking.

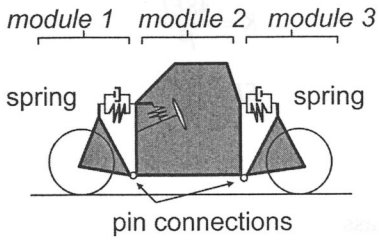

Figure 4.10 Customer evaluation mule for structural solidness.

We can now use this target of *22–25 Hz* for the vehicle bending frequency to establish a body bending stiffness target. Let us view the body structure as a uniform beam, Figure 4.11a. The primary bending frequency of a uniform beam [3] is related to its length, linear mass density, and section bending stiffness (*EI*):

$$\omega_n = \frac{22.4}{L^2}\sqrt{\frac{EIg}{w}} \qquad (4.1)$$

$$\omega_n = 22.4L^{-\left(\frac{3}{2}\right)}\sqrt{\frac{EI}{M}}$$

where:

w = Weight per unit length

M = Total mass = wL/g

ω_n = Bending resonant frequency

L = Beam length

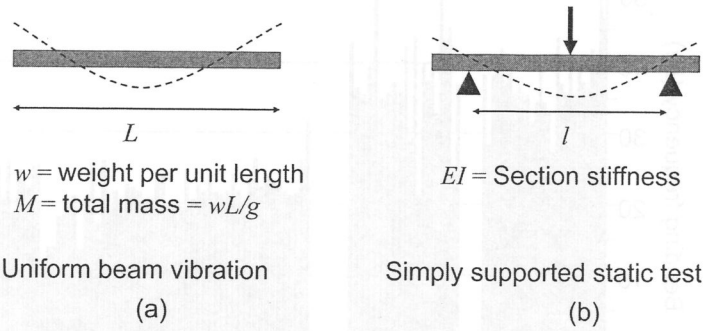

Figure 4.11 First-order model for bending frequency.

Now consider the same beam but loaded with a single static load at its center span, Figure 4.11b. The beam is supported at points representing the suspension points—the length between supports is the wheelbase. The stiffness of such a beam is related to the support length and section bending stiffness (EI):

$$K = \frac{48EI}{l^3}$$
$$EI = \frac{Kl^3}{48} \tag{4.2}$$

where:

l = Wheel base

M = Rigidly mounted mass

K = Required bending stiffness

We can now eliminate (EI) between Equations 4.1 and 4.2 by substituting Equation 4.2 for (EI) into Equation 4.1, and we are left with a relationship between bending resonant frequency and static bending stiffness, K.

$$\omega_n = 22.4L^{-\left(\frac{3}{2}\right)}\sqrt{\frac{Kl^3}{48M}}$$
$$\omega_n = \frac{22.4}{\sqrt{48}}\left(\frac{l}{L}\right)^{\frac{3}{2}}\sqrt{\frac{K}{M}} \tag{4.3}$$

where:

l = Wheel base

L = Overall length

M = Rigidly mounted mass

K = Required bending stiffness of the body

ω_n = Desired bending resonant frequency for the vehicle (rad/sec)

Thus given a target for vehicle bending frequency, ω_n, the lengths l and L, and the rigidly mounted mass, M, we can identify the required H point bending stiffness, K. Rigidly attached masses are those which participate fully in the vibration of the body structure and do not include those masses which are isolated with bushings. For preliminary design, the rigidly attached mass is taken as *0.4* to *0.6* times the vehicle curb mass, with the larger value relating to luxury vehicles.

Example: Developing a bending stiffness requirement

Consider a midsize vehicle in the early design stage having the following numerical values for key parameters:

$$l = 2700\ mm$$

$$L = 4550\ mm$$

M = rigidly attached mass ~*0.4* to *0.6* times curb mass. For this case, the lower value for $M = 0.4 \times 1446 = 578\ kg$ and the upper value for $M = 0.6 \times 1446 = 868\ kg$

We desire to establish the bending stiffness requirement that would allow us to achieve a bending resonance for the vehicle in the *22–25 Hz* range. Substituting numerical values into Equation 4.3 we can investigate the relationship between resonant frequency, rigidly mounted mass, and bending stiffness. This analysis indicates that a bending stiffness requirement of approximately *7000 N/mm* will achieve the desired *22–25 Hz* vehicle frequency, Figure 4.12.

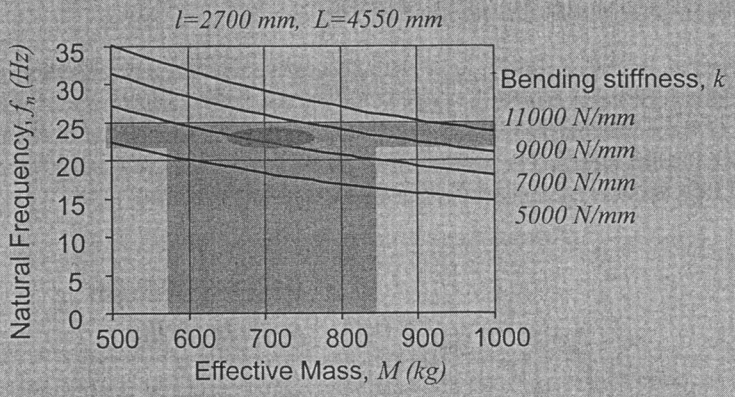

Figure 4.12 First order estimation of bending stiffness.

Note that the bending stiffness requirement for a specific vehicle depends on the parameters in Equation 4.3. Thus vehicles which have higher mass loading (highly optioned luxury cars for example) or cars with long overall length (four-door sedans vs. two-seat sport coupes, for example) will require higher static bending stiffness to achieve the same frequency target. Benchmark data for bending stiffness is shown in Figure 4.13.

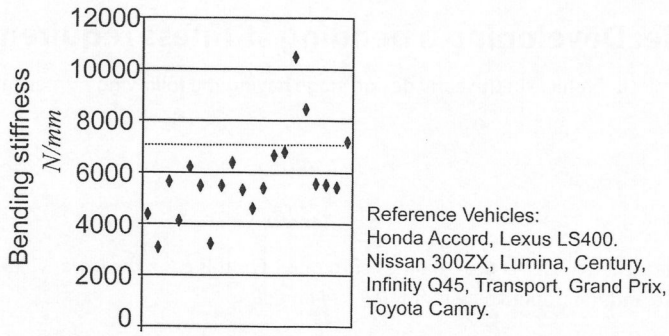

Figure 4.13 Bending stiffness test and benchmarking. (Courtesy of the American Iron and Steel Institute, UltraLight Steel Auto Body)

In addition to adequate bending stiffness being important for structural feel, a high bending stiffness is also significant in reducing the relative deformations which cause squeaks and rattles during normal use.

To summarize, we have shown how both strength and stiffness requirements may be established for body bending. Typical values for these requirements are shown in Figure 4.14 for a midsize vehicle. We will now look at the design of body structure to meet these requirements. The next section treats design for the strength requirement, followed by a section on design for the stiffness requirement.

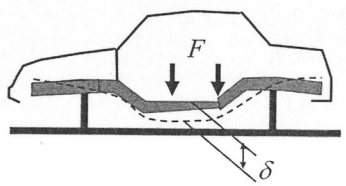

Bending strength

nominal value

$F = 6680\ N$

no permanent deformation

Bending stiffness

nominal value

$K = 7000\ N/mm$

Figure 4.14 Typical bending requirements: Midsize vehicle.

4.3 Internal Loads During Global Bending: Load Path Analysis

First we will consider the design of structure to meet the body strength requirement. Our objective is to understand how the global body requirement flows down to loads on structure elements such as the beams in the side frame. Once we have loads on individual beams, we can then use the techniques discussed in Chapter 3 to design the appropriate beam sections.

We will idealize the body as a set of structural surface and bar elements. A structural surface [4] is a flat element which is loaded in shear along its edges. Loads normal to the surface, or bending moments, cannot be reacted, Figure 4.15a. A bar element is a linear element which can only react loads along its axis, either end loads or shearing loads along the length, Figure 4.15b. Using only structural surfaces and bars, we can construct the model for the auto body shown in Figure 4.16.

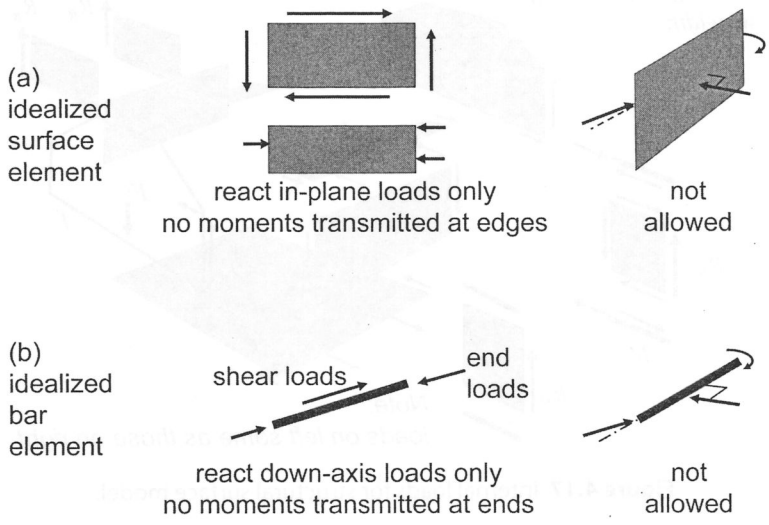

Figure 4.15 Idealized structural elements.

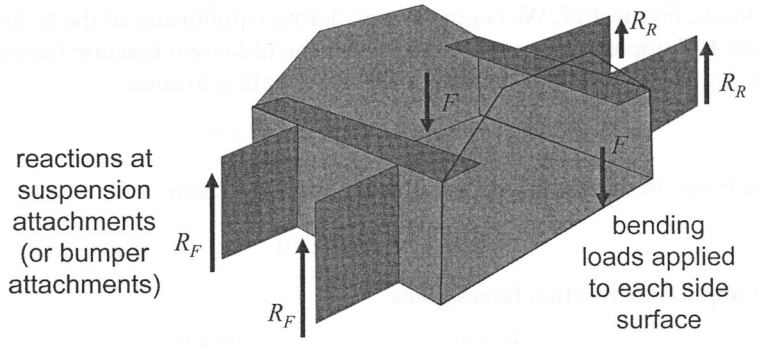

Figure 4.16 Structural surface and bar body model.

We can now load this model as in an H point bending test by applying a downward load F in the plane of the side structural surface, Figure 4.16, and supporting the structure with edge loads R_F and R_R. Note that this loading is symmetrical side-to-side.

The magnitude of the applied load, F, represents the bending strength requirement which we would like to react with just a small amount of permanent deformation. We would like to know the loads that are applied to each of the structural elements, *a* through *f*, in Figure 4.17. Once we know these maximum internal loads, we can then design each element for strength. This process is known as flow down of requirements, from a global requirement to a requirement for a specific structural element.

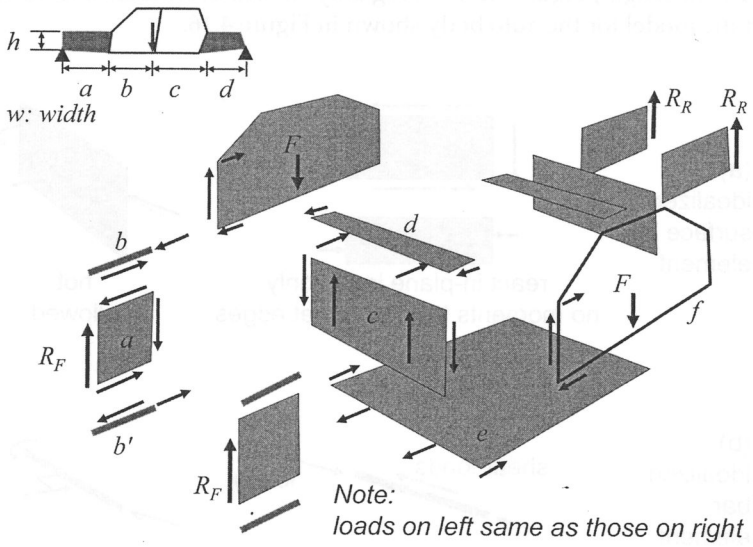

Figure 4.17 Internal loads for structural surface model.

By exploding the structure [5], we can use free-body analysis to identify these element loads, Figure 4.17. We begin by considering equilibrium of the full body, (see Figure 4.17 upper left corner) and solve for the unknown reaction forces R_R and R_F. Summing moments about the front axle and equating to zero:

$$2R_R(a+b+c+d)-2F(a+b)=0$$

Summing forces in the vertical direction and equating to zero:

$$2R_F+2R_R-2F=0$$

Solving these for the reaction forces gives:

$$R_F=F\frac{(c+d)}{(a+b+c+d)},\qquad R_R=F\frac{(a+b)}{(a+b+c+d)} \tag{4.4}$$

Next we will put each element, *a* through *f*, into static equilibrium beginning with an element, *a*, which is loaded by one of the reaction forces.

Looking at the exploded structure we can begin by putting the structural surface *a* into equilibrium. Remembering that we can only have shear loads along edges, this panel has the known reaction force R_F along the front edge (and $-R_F$ along the rear edge by static equilibrium in the vertical direction). An unknown load Q acts on the top and bottom edges, as shown in Figure 4.18. Summing moments about point o and equating to zero:

$$\begin{aligned} Qh - R_F a &= 0 \\ Q &= R_F \frac{a}{h} \end{aligned} \tag{4.5}$$

Now taking each element, *a* through *f*, Figure 4.17, we can use equilibrium to determine all internal loads.

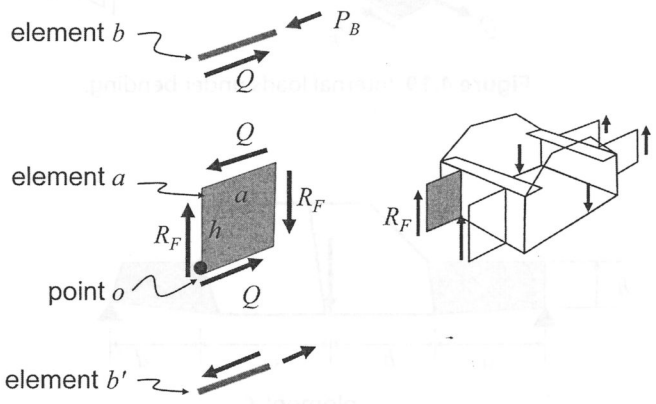

Figure 4.18 Internal loads on motor compartment panel.

For the upper bar element, *b*, Figure 4.18, the applied shearing load is Q from element a, and we can have an end force P_B. Equilibrium along the horizontal direction gives $P_B = Q$. Similarly, for element *b´*, we find $P_B' = Q$.

For the dash panel, *c*, Figure 4.19a, the applied loads are R_F from element *a*, with reactions at the outer edges of P_C, so $P_C = R_F$. The cowl panel, *d*, Figure 4.19b, is loaded by the upper bar, *b*, and has reaction loads, P_D, at its edges, so $P_D = Q$. The front portion of the floor pan, *e*, Figure 4.19c, is loaded on each side by the lower bar, *b´*, with load Q and by the side panel, *f*, by an equal and opposite load, $P_E = Q$.

Finally, looking at the side frame, structural surface *f*, Figure 4.20, we have the vertical load R_F from the dash, Q rearward at the belt line from the cowl panel, Q forward at the base of the front hinge pillar from the floor, and similar loads from the panels at the rear of the vehicle.

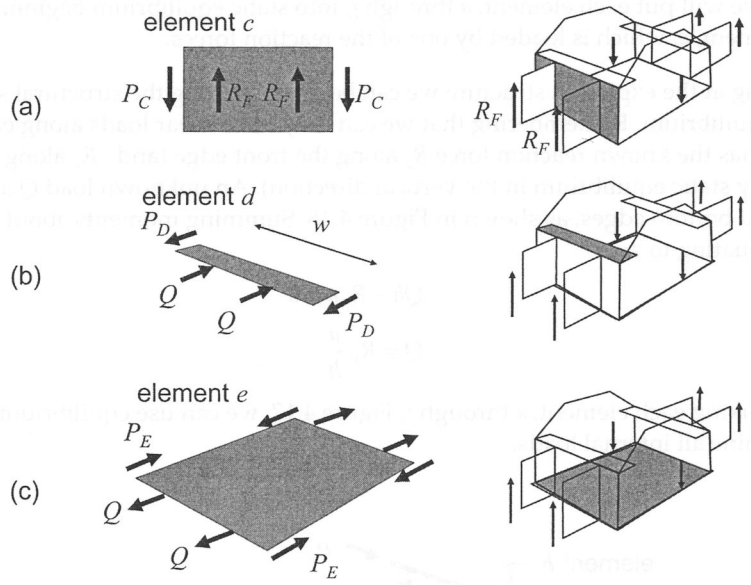

Figure 4.19 Internal loads under bending.

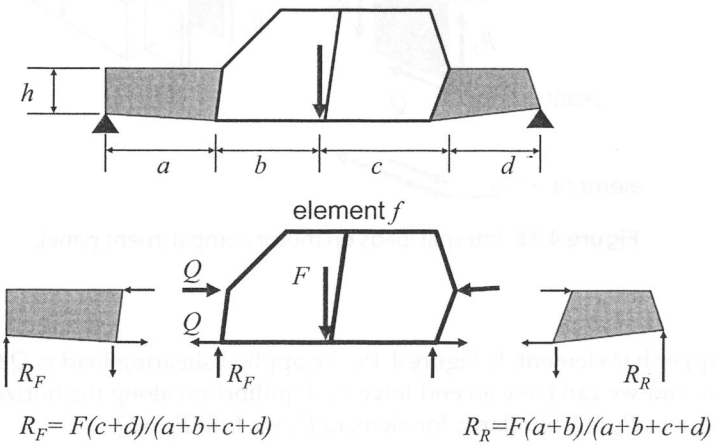

Figure 4.20 Free-body of side frame during vehicle bending.

Figure 4.21 summarizes the results for these equilibrium analyses. We have identified the load paths and loads resulting from the bending strength requirement for each element of the body. Each element must be capable of reacting the loads shown without excessive permanent deformation for the overall body structure to meet the bending strength requirement. Let us look at three of these structural subsystems in more detail to see how this information can be used in design.

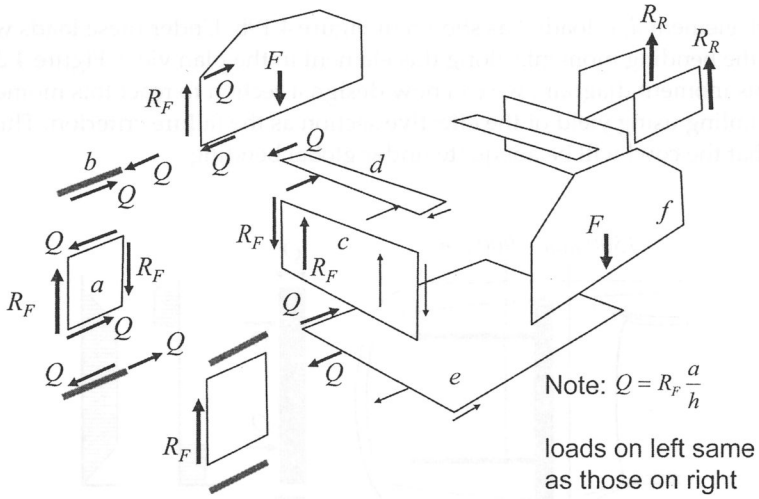

Figure 4.21 Summary: Internal loads for structural surface model.

The motor compartment side panel, element *a*, is loaded by the shearing loads shown in Figure 4.22a. This panel must react these loads in a bending strength test. However, this high, thin panel can be prone to elastic plate buckling under this loading condition, Figure 4.22b. Using the principles developed in Chapter 3, we can look at ways to increase the shear buckling critical stress. One mass-effective method is to add ribs to reduce the width of the buckling plate, Figure 4.22c.

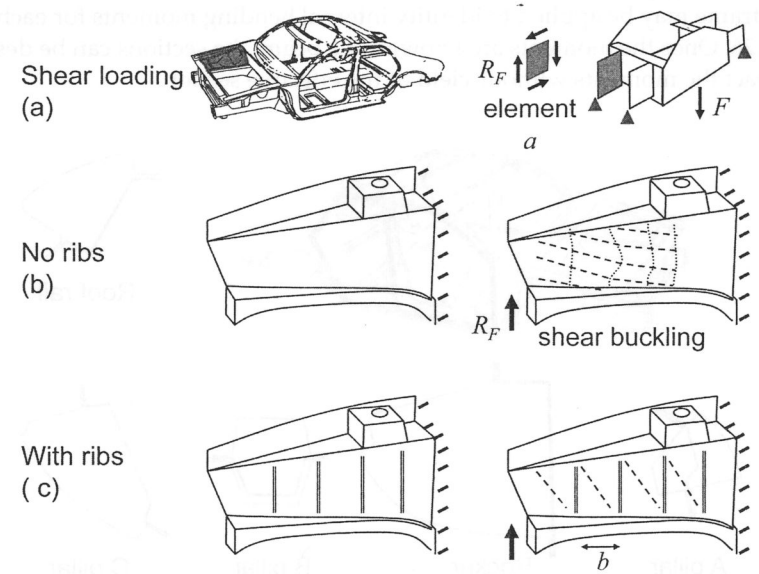

Figure 4.22 Buckling of motor compartment side panel.

The cowl, element *d*, is loaded as shown in Figure 4.19b. Under these loads we can identify the bending moments along this element in the plan view, Figure 4.23. Given this moment diagram, we can now design a section to react this moment without failing using yield of the effective section as the failure criterion. This will ensure that the cowl will be adequate under global bending.

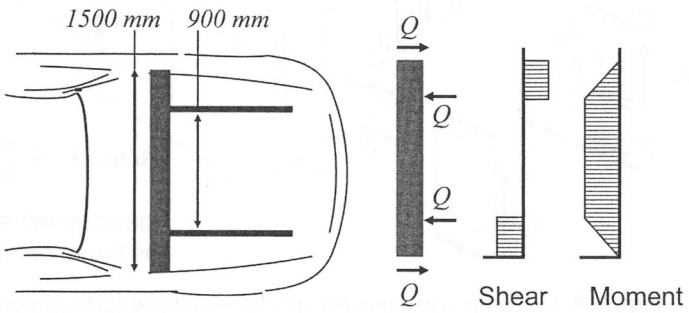

Figure 4.23 Loads on cowl surface during bending.

Finally, consider the side frame element *f*, loaded as shown in the bending test, Figure 4.20. This element is made of several beams: front hinge pillar, A pillar, roof rail, B pillar, C pillar, and rocker, Figure 4.24. Our objective is now to see what moments are applied to each beam by these loads so that we may design the beam sections. As a framework of beams, this structural subsystem is statically indeterminate; that is, we cannot use equilibrium equations only to determine the moments in each beam. The moments also depend on the relative stiffness of each of the beams. Using the loading shown in Figure 4.25, a small finite element model of the side frame may be applied to identify internal bending moments for each beam, Figure 4.26. Once the moments are known for a beam, the sections can be designed which react the moments without yield of the effective section.

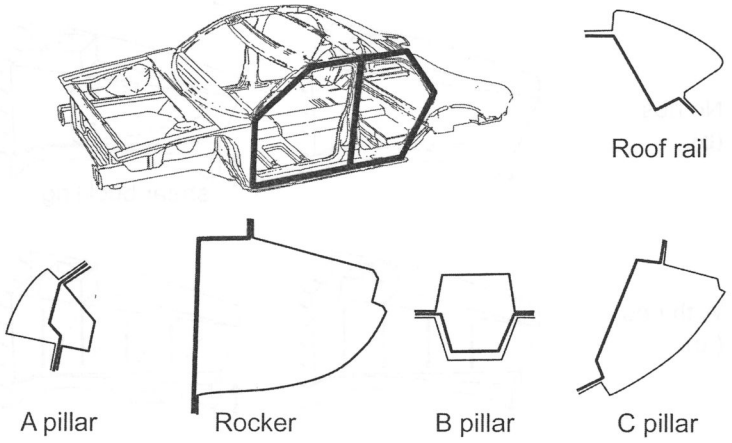

Figure 4.24 Side frame beams.

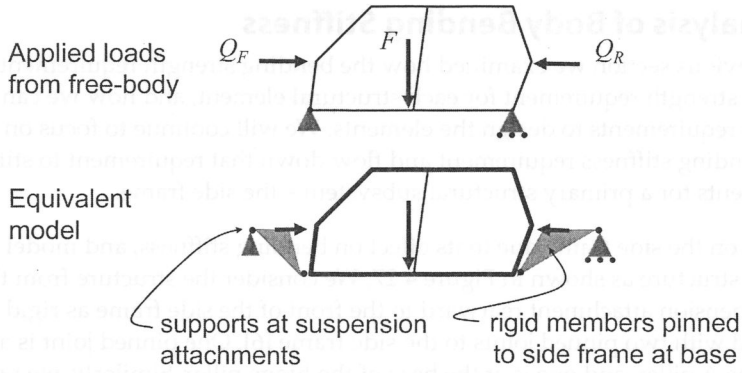

Figure 4.25 Side frame planar beam model.

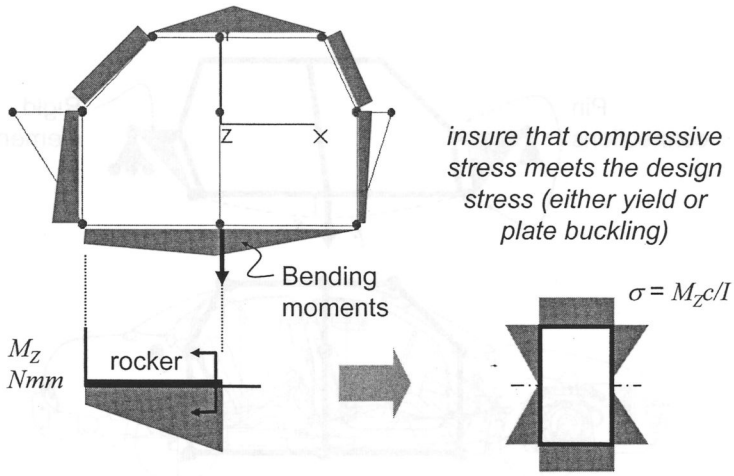

Figure 4.26 Finite element analysis for internal loads.

4.3.1 Summary: Bending strength

In this section, we have shown how the applied loads in the global bending strength test can be flowed down to the loads on each individual structural subsystem of the body. To accomplish this flow down of load requirements, we used a highly idealized body structure of simple structural surfaces and bar elements, Figure 4.21. We set each element into static equilibrium to find the internal element loads. Then, knowing the subsystem loads, we showed how the section design principles developed in the previous chapter can be used to find the appropriate sections to react these loads. We have thus gone from a strength requirement on the body system to ensuring the strength of each structural element in the body under bending.

4.4 Analysis of Body Bending Stiffness

In the previous section we examined how the bending strength requirement implies a strength requirement for each structural element, and how we can use these requirements to design the elements. We will continue to focus on the global bending stiffness requirement and flow down that requirement to stiffness requirements for a primary structural subsystem—the side frame.

We focus on the side frame due to its effect on bending stiffness, and model the body structure as shown in Figure 4.27. We consider the structure from the front suspension attachment rearward to the front of the side frame as rigid and connected with two pinned joints to the side frame [6]. One pinned joint is at the base of the A pillar, and one is at the base of the hinge pillar. Similarly, we use a rigid element from the rear suspension attachment forward to the side frame and attached in the same way as shown in Figure 4.27. With this configuration, the side frame is loaded as in our earlier free-body shown in Figure 4.20.

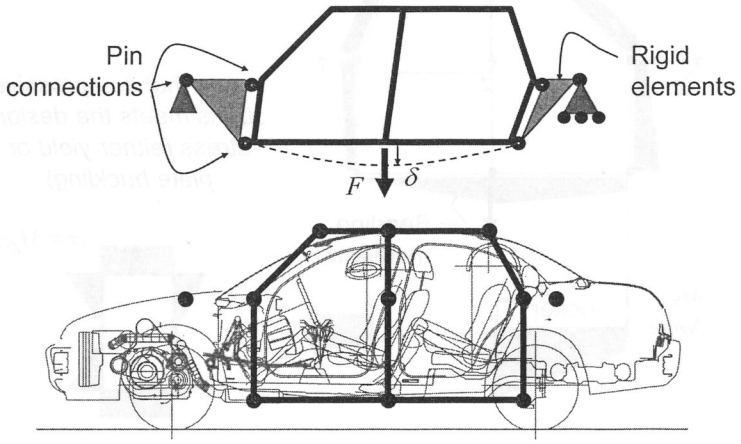

Figure 4.27 Very basic side frame finite element model. (Courtesy of the American Iron and Steel Institute, UltraLight Steel Auto Body)

We will follow the design procedure shown in Figure 4.28. Beginning with the global bending stiffness requirement, we will create a side frame design concept by making an initial estimate for the section size of each of the beam elements in the side frame. We will then predict the bending stiffness performance using a finite element model based on Figure 4.27. We will then compare the estimated performance to the required stiffness and adjust the beam sizes until the requirement is met at acceptable mass.

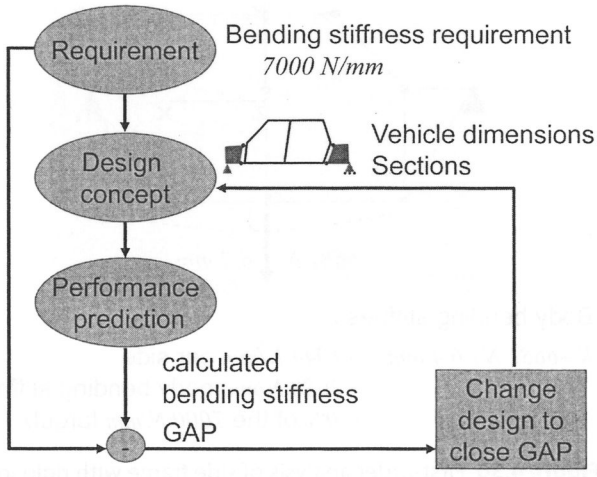

Figure 4.28 Systems design procedure.

Consider example data for this model. Figure 4.29 shows the initial guess for beam section size—height, width, and thickness for the rectangular sections. These beams are used in the simple finite element model [7] shown in Figure 4.30, in which each beam is rigidly connected to adjacent beams at a node point. The model is restrained at the front suspension attachment point by restraining deflection in all three directions (but allowing rotation about all three axes), and restrained at the rear suspension attachment point in the vertical direction and out-of-plane direction. A downward load is applied at the node where the B pillar attaches to the rocker, simulating the H point bending load, Figure 4.30.

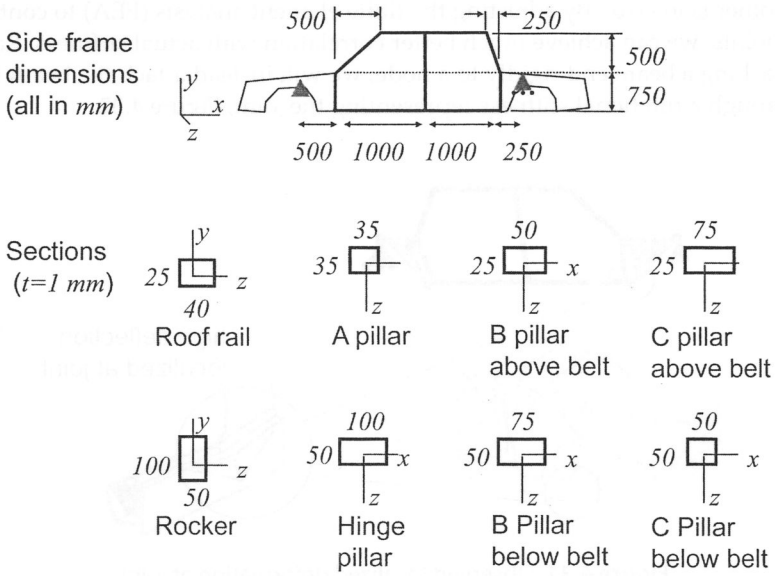

Figure 4.29 Example data for side frame model.

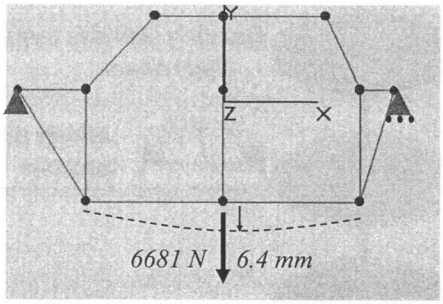

Body bending stiffness:

K=6681 N / 6.4 mm *=1044 N/mm* per side
=2088 N/mm body bending stiffness
(30% of the *7000 N/mm* target*)*

Figure 4.30 First-order analysis of side frame with rigid joints.

The result of this analysis is the deflected shape of the side frame. By taking the ratio of the applied load to the deflection at the node of load application, we can calculate the bending stiffness for the side frame, Figure 4.30.

4.4.1 Importance of joint flexibility

If we were to compare the actual stiffness to what we have predicted with this model, we would find the predicted stiffness is approximately twice the actual. We have neglected a very important physical behavior of the thin-walled beam sections: whenever two or more thin-walled beams are joined, there is considerable localized deformation, Figure 4.31. This localized deflection has the effect of a flexible joint between the beams [8]. Thus, our assumption that the beams are rigidly connected to each other is in error. By adjusting the finite element analysis (FEA) to contain flexible joints, we can achieve much better correlation with actual stiffness. Rather than attaching a beam end rigidly to a node, we will instead attach the beam to a node through a rotational stiffness representing the joint, Figure 4.32.

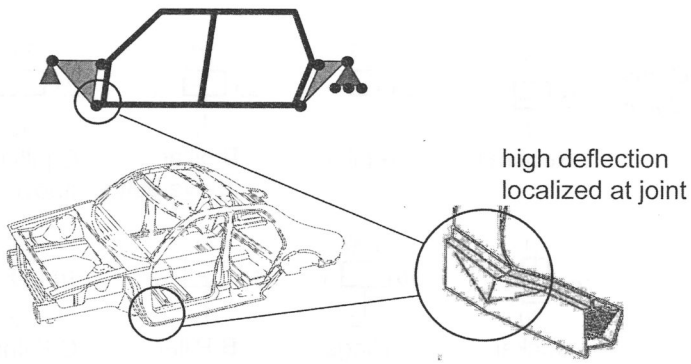

Figure 4.31 Observed localized deformation at joint.

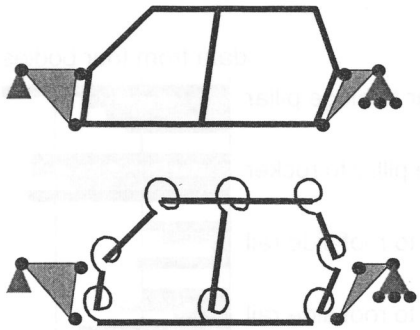

Figure 4.32 Modified model with joint flexibility.

The rotational stiffness value is determined by extracting the physical joint from the body structure, restraining all beam connections except one, and applying a moment at that beam connection, Figure 4.33. The resulting rotational deflection is measured and a moment-rotational angle curve plotted. The slope of this curve is the joint stiffness. Benchmark data for side frame joints of four vehicles are shown in Figure 4.34, and joint stiffnesses for five different joints are compared.

The absolute value for joint stiffness is somewhat difficult to interpret. For example, is a joint stiffness of *0.2x10⁶ Nm/rad (1.77x10⁶ in lb/rad)* a very stiff or very flexible joint? To answer this question, it is helpful to compare the joint stiffness to the bending stiffness of the beam to which it is attached, Figure 4.35a. We can then define joint efficiency, *f*, as the ratio of the combined stiffness of the beam with joint to the stiffness of the beam alone (assuming a rigid joint).

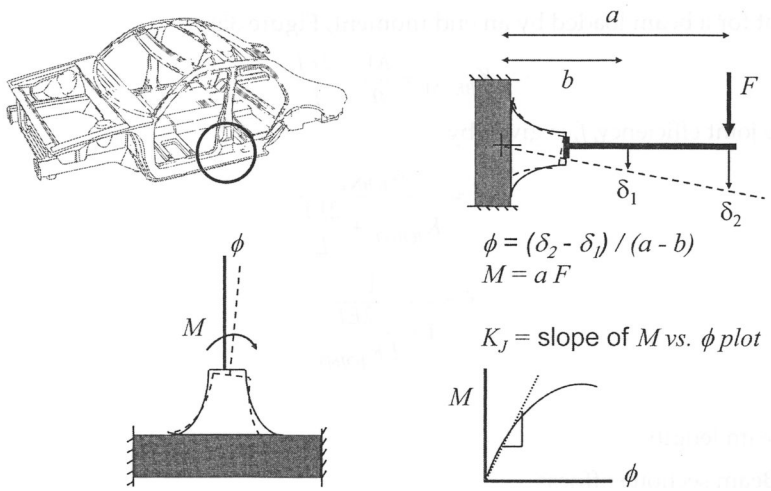

Figure 4.33 Measuring joint rates.

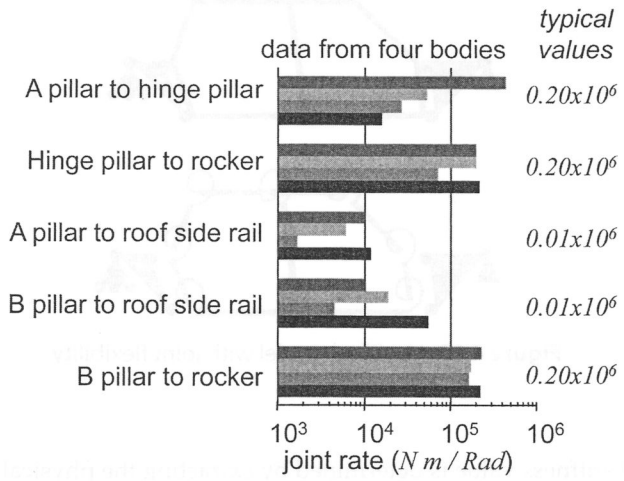

Figure 4.34 Typical joint rates for side view.

$$f = \frac{K_{BEAM\&JOINT\ SYSTEM}}{K_{BEAM}} \tag{4.6}$$

Since the beam stiffness and joint stiffness are in series,

$$K_{BEAM\&JOINT\ SYSTEM} = \frac{K_{JOINT}K_{BEAM}}{K_{JOINT} + K_{BEAM}} \tag{4.7}$$

Substituting Equation 4.7 into 4.6 gives,

$$f = \frac{K_{JOINT}}{K_{JOINT} + K_{BEAM}}$$

Note that for a beam loaded by an end moment, Figure 35b,

$$K_{BEAM} = \frac{M}{\theta} = \frac{2EI}{L} \tag{4.8}$$

Then the joint efficiency, f, is given by

$$f = \frac{K_{JOINT}}{K_{JOINT} + \frac{2EI}{L}}$$

$$f = \frac{1}{1 + \frac{2EI}{LK_{JOINT}}} \tag{4.9}$$

where:

L = Beam length

EI = Beam section stiffness

K_{JOINT} = Joint stiffness

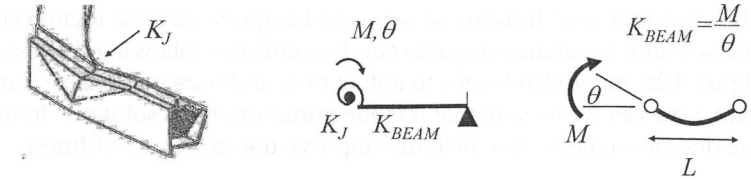

Rocker beam to hinge pillar joint K_J

Beam & joint system stiffness (a)

Beam stiffness alone (b)

Figure 4.35 Joint efficiency.

When the joint stiffness, K_{JOINT}, is much larger than the beam stiffness, $(2EI/L)$, the denominator of Equation 4.9 is approximately one, and the efficiency approaches *100%*. Thus a *100%* efficient joint would be rigid with all of the beam stiffness being utilized. A very low efficiency indicates most of the deformation of the beam-joint system is caused by the joint deformation.

Example: Joint efficiency

Consider the steel rocker beam from the side-frame model of Figure 4.29. To the rocker, we will place a typical joint for the Hinge Pillar-to-rocker joint, Figure 4.34. With these assumptions, we have

$I=4.15x10^5\ mm^4$ (computed from the values $h=100\ mm$, $w=50\ mm$, $t=1\ mm$)

$K_{JOINT}=0.2x10^6\ Nm/rad=0.2x10^9\ Nmm/rad$ from Figure 4.34

$L=1000\ mm$, the length of the rocker beam from Figure 4.29

Inserting these values into Equation 4.9 gives

$$f=\frac{1}{1+\frac{2(207000N/mm^2)(4.15x10^5 mm^4)}{(1000mm)(0.2x10^9\ Nmm/rad)}}$$

$$f=0.537$$

So for this beam-joint system, the presence of the joint reduces the stiffness to approximately one half that of the beam.

Consider again our side-frame model of Figure 4.29. We now apply reasonable joint stiffnesses to three of the joints, Figure 4.36 and re-run the FEA. The resulting side frame stiffness, Figure 4.37, is *83%* of that with rigid joints, Figure 4.30, and is in better agreement with physically measured values. We are now content that we have a valid model to predict side frame stiffness given an initial guess at beam section sizes. What if our initial guess does not give a stiffness which meets the

required bending stiffness? Intuitively, we would begin to increase section sizes or joint stiffnesses until we attain adequate bending stiffness following the iterative loop of Figure 4.28. But which beams to adjust first, and once we achieve the requirement, how can we be sure that it is the minimum mass solution? In the next section, we describe a means to efficiently improve the structure's stiffness.

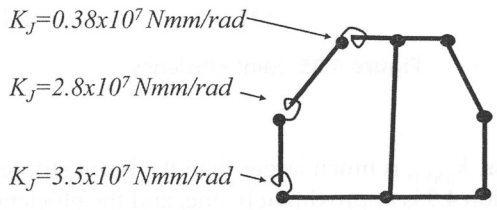

Figure 4.36 Model with flexible joints.

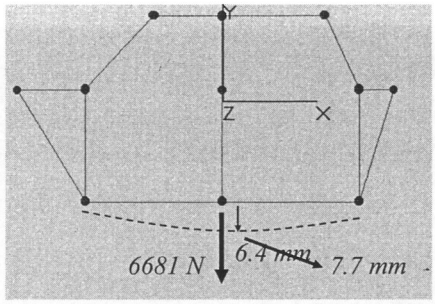

Body bending stiffness= ~~2088 N/mm~~ 1735 N/mm

Figure 4.37 Effect of joint stiffness on bending stiffness.

4.4.2 Strain energy and stiffness

As the bending load is applied to the body structure, the structure deflects at the point of load application. As the applied force moves through this displacement, it does work. This external work is stored as strain energy in each of the structural elements as they deform under the load. The strain energy in a structural element may be calculated if we know the applied moments.

For example, in Figure 4.38 the strain energy of an end-loaded beam is developed as a function of the end moments on the beam, resulting in the relationship:

$$e_{BEAM} = \frac{L}{6EI}(M_1^2 + M_1M_2 + M_2^2) \tag{4.10}$$

where:

L = Beam length

EI = Section stiffness

$M_{1,2}$ = Applied moment at each end

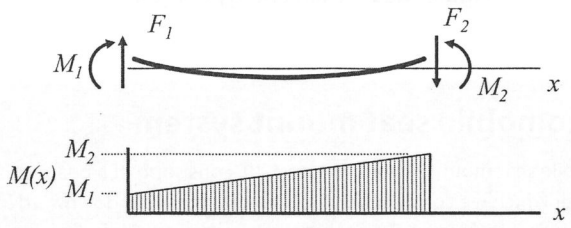

For end loaded beam $$M(x) = M_1 + \frac{(M_2 - M_1)}{L}x$$

Strain energy for beam $$e = \int_0^L \frac{My''}{2}dx = \int_0^L \frac{M^2}{2EI}dx$$

$$e = \frac{L}{6EI}(M_1^2 + M_1M_2 + M_2^2)$$

Figure 4.38 Strain energy of a beam loaded at ends.

The strain energy for a joint of stiffness K_{JOINT}, Figure 4.39, with applied moment, M, and resulting angle of rotation, ϕ, is:

$$e = \frac{M\phi}{2} = \frac{M^2}{2K_{JOINT}}$$
$$e = \frac{\phi^2 K_{JOINT}}{2} \qquad (4.11)$$

where:

K_{JOINT} = Joint stiffness

M = Applied moment at each end

ϕ = Deflection angle (rad)

Thus, knowing the moment applied to a structural element—either a beam or joint—we can identify the strain energy stored in it by using Equation 4.10 or 4.11.

We can now answer the question of which beam or joint to improve first to meet the body bending stiffness requirement most efficiently:

To improve the stiffness of a structural system, increase the performance of the structural element with the highest fraction of strain energy.

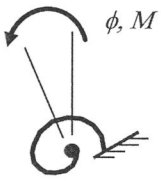

$$e = \frac{M\phi}{2} = \frac{M^2}{2K_J} = \frac{\phi^2 K_J}{2}$$

Figure 4.39 Strain energy of a joint.

Example: Automobile seat mount system

Consider the automobile seat mount system, Figure 4.40, consisting of a beam connected by a flexible joint to a rocker which we consider as rigid. The seat applies a downward load and we are interested in the vertical stiffness. Assume that the current system design does not meet the stiffness requirement, and we wish to know which element to change—the beam or the joint—to increase the stiffness of the system. Using the values given in Figure 4.40 we can calculate the strain energy in each element.

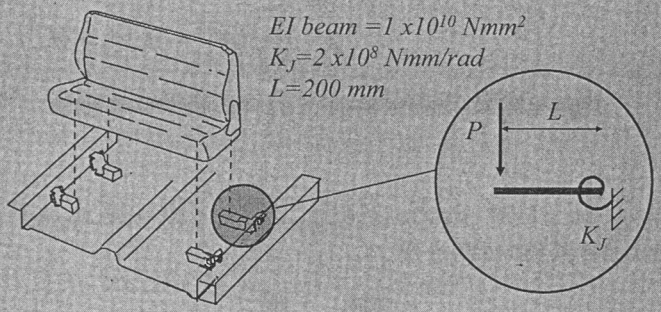

Figure 4.40 Seat mount system.

The strain energy in the beam using Equation 4.10 is

$$e_{BEAM} = \frac{200mm}{6(1x10^{10}\,Nmm^2)}(M_2^2) = 3.33x10^{-9}M_2^2$$

where:

M_2 = Moment at the connection with the rocker

The strain energy in the joint using Equation 4.11 is

$$e_{JOINT} = \frac{M_2^2}{2(2x10^8\,Nmm/rad)} = 2.5x10^{-9}M_2^2$$

Since the strain energy in the beam is greater than that in the joint, an incremental change in beam stiffness will have a larger effect on overall system stiffness than an incremental change in joint stiffness.

While the use of strain energy in this very simple example is not essential, in more complex systems such as the side frame it is much more difficult to identify which beam or joint to improve. Strain energy for these complex structures becomes a critical tool for iterative improvement of the structure. For more complex structural systems, strain energy can be calculated, using the FEA model which evaluates Equations 4.10 and 4.11, for each beam and joint within the software.

Example: Side frame design to meet the bending requirement

We continue with the side frame model presented first in Figure 4.27. The initial guess at beam section sizes is shown in Figure 4.29, and the predicted bending stiffness for these beams with joints is shown in Figure 4.37. This predicted stiffness does not meet the bending requirement of $K \geq 7000$ N/mm, Figure 14. Now consider another result of the FEA, Figure 4.41, which is the strain energy percent in each element. To improve side-frame bending stiffness most efficiently, we increase the beam section with the highest strain energy—in this case, the front rocker beam. We increase the beam height, the most mass-effective way to increase moment of inertia, and re-run the FEA. This will result in a new estimate for stiffness and also a different strain energy distribution. We continue this process in an iterative fashion until we improve the stiffness performance to meet the requirement. This process requires several iterations and is often automated within the FEA software.

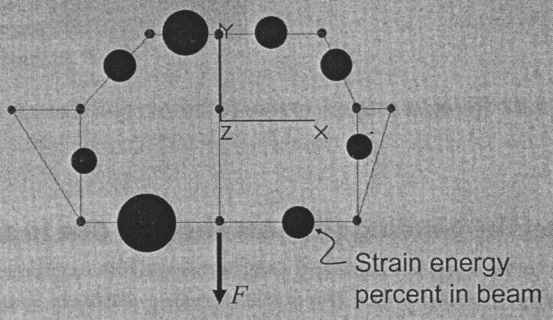

Figure 4.41 Strain energy in side frame.

Once we have sized the sections to meet the bending stiffness requirement, we consider the bending strength requirement. We follow the procedure shown in Figure 4.42 and look at the maximum stress in each beam to ensure the stress is within the design stress level. With thin-wall design, careful attention is given to the compressive stresses to ensure they are within the plate buckling stress limits. If stress is greater than the design stress we have a choice of:

1. Increasing the buckling design stress by inhibiting elastic plate buckling using the methods described in Chapter 3
2. Choosing a material with increased yield when buckling is not the limiting failure condition
3. Reducing the stress by increasing the section properties.

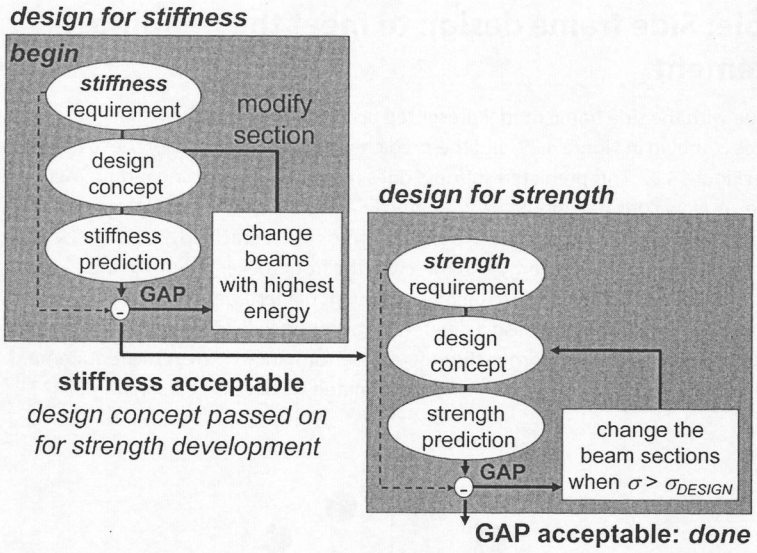

Figure 4.42 Iterative process to meet stiffness and strength requirements.

4.4.3 Note on the bending stiffness changes due to side doors

The model we have used for bending performance has neglected side doors. It has been shown experimentally that the static bending stiffness is unchanged with or without doors attached. To understand this non-obvious behavior, consider the deflected shape of the side frame with an idealized door in place, Figure 4.43. To add to the global bending stiffness, the door system must generate the loads shown at the hinges and latch. However, current designs for the hinge and latch do not have sufficient stiffness to generate these loads. Alternative designs for door attachment can provide this stiffness. For example, Figure 4.44 shows a highly rigid hinge attachment design [9].

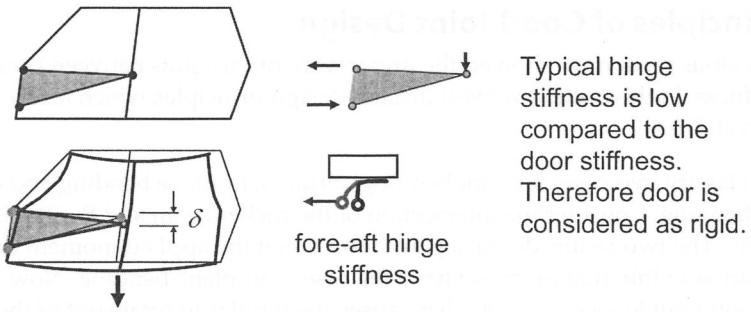

Figure 4.43 Effect of door on body bending stiffness.

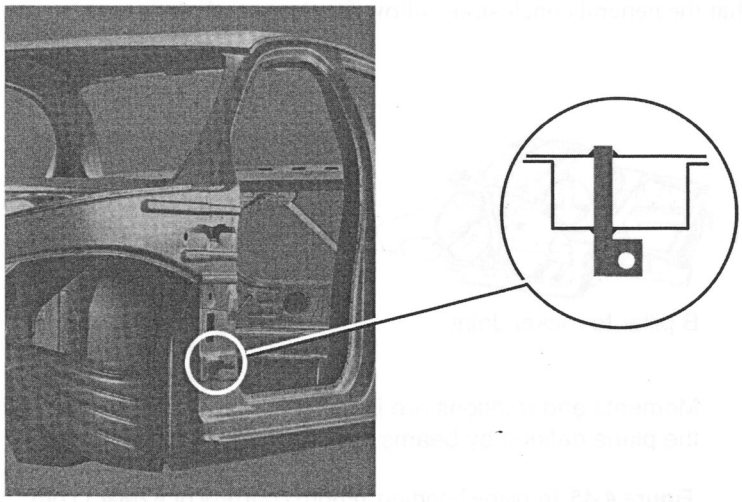

Figure 4.44 Through-section door hinge attachment. (Courtesy of the American Iron and Steel Institute, UltraLight Steel Auto Body)

4.4.4 Summary: Bending stiffness

In this section, we have shown how the global bending stiffness requirement can be flowed down to identify the required properties of individual beams and joints. We used a simple Finite Element Analysis of the side frame to predict deflections and also element strain energy. Strain energy informed us regarding which beams have the most influence on global bending stiffness. We have also shown how joint stiffness plays an important role in global bending stiffness performance.

Often the structural element which most influences global bending stiffness is a joint rather than a beam element. In the following section, we look at principles of joint design for stiffness.

4.5 Principles of Good Joint Design

In the previous section we showed the importance of the joints between beams to body stiffness. In this section we will discuss design principles which result in joints with high stiffness.

First, we classify two cases for joint bending stiffness: in-plane bending and out-of-plane bending. Consider the intersection of the rocker beam and B pillar beam, Figure 4.45. The two beams define a plane, and when the applied moment causes beam rotation within that plane we have the case of in-plane bending. Now consider the same joint but loaded in a way that causes the B pillar to rotate out of the plane containing the two beams, Figure 4.46. This is the out-of-plane bending case. In most instances, in-plane bending joint stiffness is of interest under global body bending, while the out-of-plane bending joint stiffness is of interest under global body torsion. In the following, we will focus on design principles for in-plane bending but realize that the general conclusions follow for the out-of-plane case.

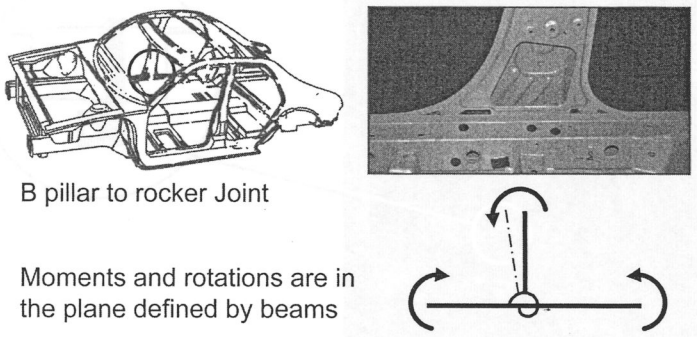

Figure 4.45 In-plane bending. (Photo courtesy of A2Mac1.com Automotive Benchmarking)

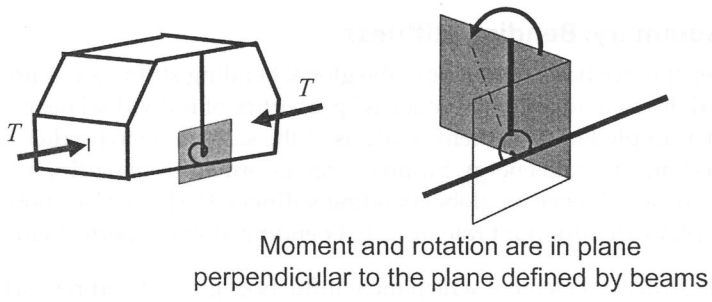

Figure 4.46 Out-of-plane bending.

We will develop principles for stiff joints by first looking at a case of an undesirable flexible joint, that is one with much local deformation where the beams join. In this simplified joint, two beams with rectangular section join in a planar T shape similar to the B pillar to rocker joint, Figure 4.47. The section width for the B pillar is smaller than the width of the rocker section. The rocker is restrained at either end, and a rearward load is applied at the top of the B pillar beam, creating the stress distribution shown in Figure 4.48. Because we are dealing with thin-walled sections, the corners of the section have a relatively higher stress than the center of the walls. We can idealize this stress distribution by assuming that all of the stress is taken by the corners of the section, as shown in Figure 4.49. Now isolating the top surface of the rocker section and considering it as a simply supported plate, we can see that the corner loads from the B pillar are applied to the central portion of this plate, Figure 4.50. As a thin-walled plate, it has little bending rigidity to react these centrally applied normal loads, and there is considerable deformation of the plate as shown in Figure 4.51.

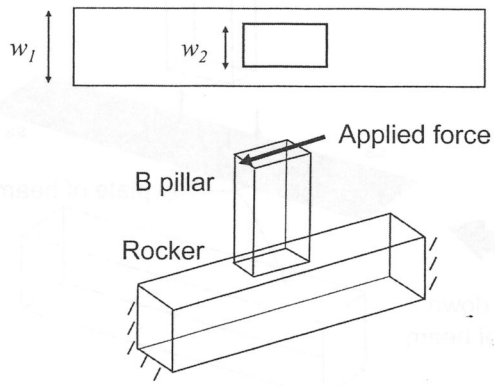

Figure 4.47 Simplified joint of thin-walled sections under in-plane bending.

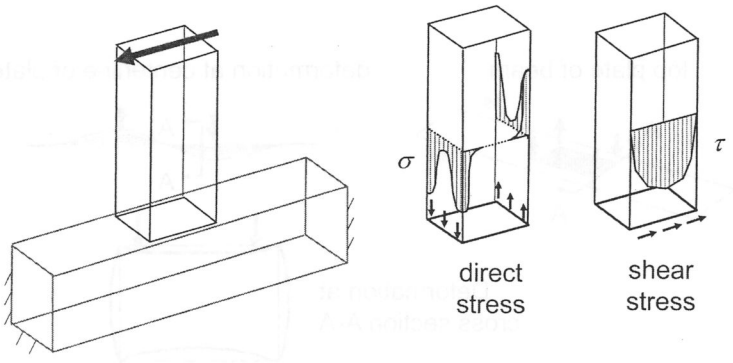

Figure 4.48 Stress distribution for loaded joint.

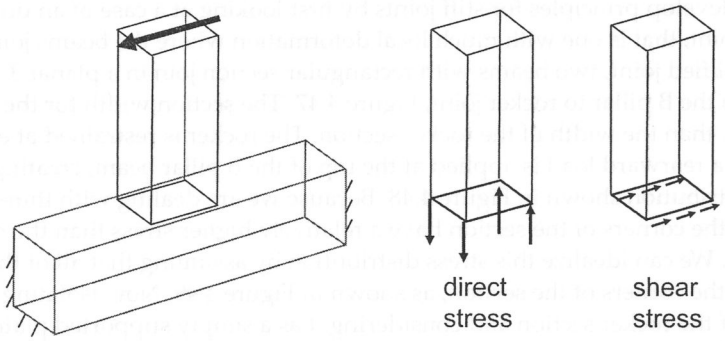

Figure 4.49 Idealized stress distribution for thin-walled section.

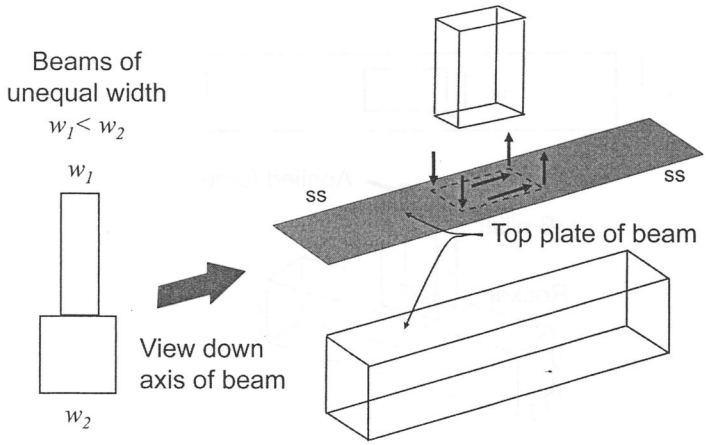

Figure 4.50 Reaction stresses generated by deforming top plate.

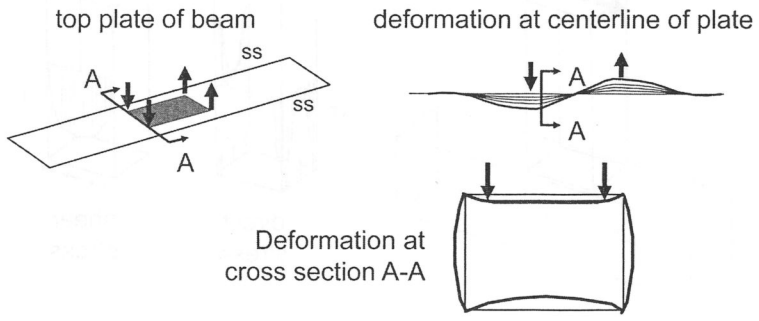

Figure 4.51 Deformation of top plate for joint with beams of unequal width.

This condition, in which a corner load from one beam normally loads a plate surface of the connecting beam, is the basis for the high joint flexibility we are trying to avoid. As an improvement to this joint configuration, consider that both beams are now of the same width, Figure 4.52. Now the corner loads from the B pillar are reacted by shearing in the side surface of the rocker. Considerably less deformation occurs under this shear action, and the joint flexibility is greatly reduced. This provides a guideline for stiff joint construction:

For high joint stiffness, the shear walls of the connected beams should be aligned at the joint and flow smoothly from one beam to another.

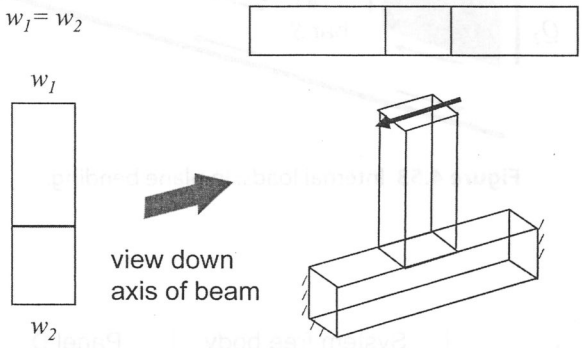

Figure 4.52 Joint with beam side walls coincident.

To better understand this improved joint configuration, consider the shear sides of the two beams. Let us model these shear walls with shear resistant members and bars and load them as shown, Figure 4.53. To understand how the applied in-plane load flows through the joint, each element can be placed into static equilibrium, Figure 4.54. This analysis shows that the applied load can be reacted efficiently by shear and compression. However, two areas must be treated carefully; the shear panel at the intersection of the beams, panel *B*, is relatively highly loaded in shear and can be prone to shear buckling. Also, the bar elements at the front and rear of the B pillar, bar S_3 and S_4, are relatively highly loaded in compression and are also prone to compressive buckling. One means to solve both of these concerns is by using the rib pattern shown in Figure 4.55a. The V rib pattern increases the shear buckling stress of the panel, while the vertical ribs provide a path for the compressive load. Examining Figure 4.54, note that the corner force, X_D, acting on bar S_3 is reduced as the span, b, is increased; $X_D = hF/b$. One means to increase this span is to provide a filleted transition, as shown in Figure 4.55b.

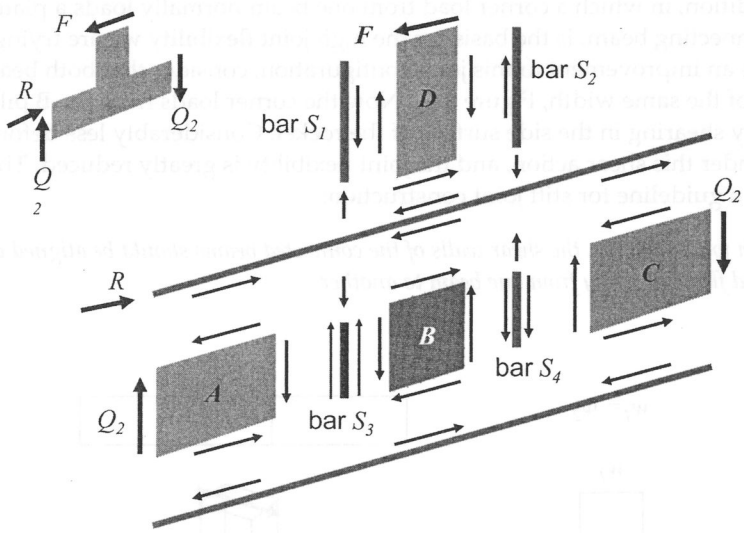

Figure 4.53 Internal loads: In plane bending.

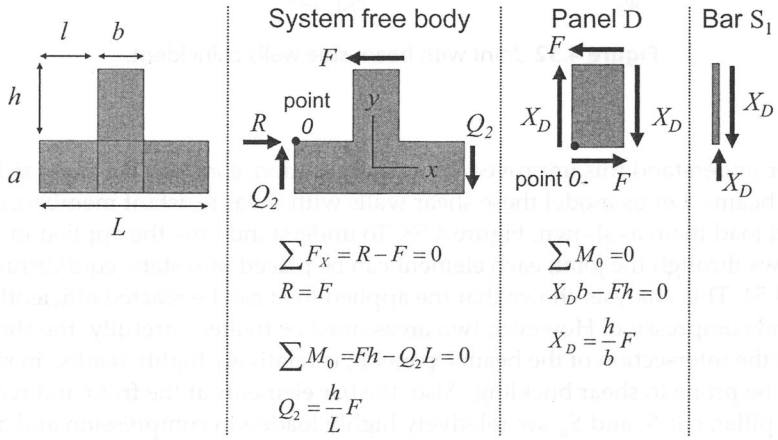

Figure 4.54a Free body diagram: In plane bending.

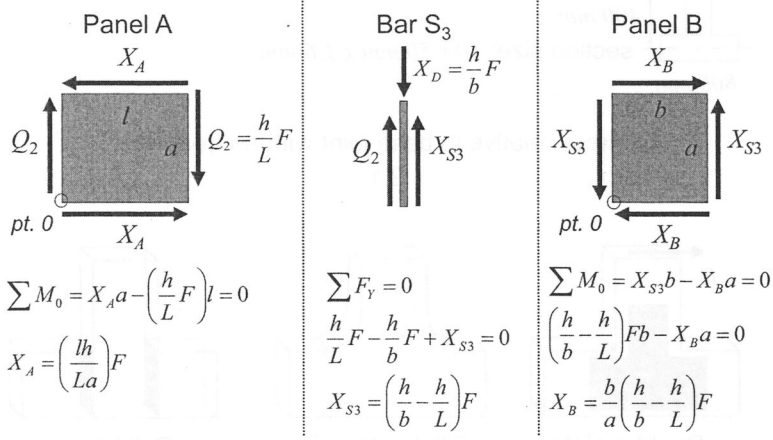

Figure 4.54b Free body diagram: In plane bending.

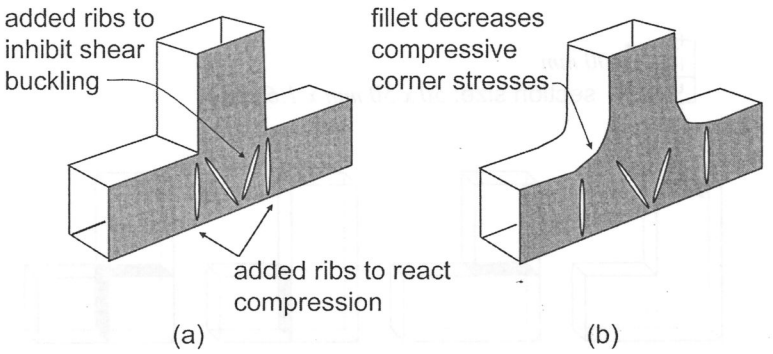

Figure 4.55 Modification to joint shear wall.

Figure 4.56 shows experimental data for in-plane bending stiffness of three alternatives to the untreated planar T joint we have been analyzing [10]. A doubler plate over the shear wall, Figure 4.56a, inhibits shear buckling, although with some mass penalty. A filleted transition, Figure 4.56b, reduces the forces applied by the corners by increasing the distance between the corner forces. Finally, by adding a bulkhead under the upper section corners, Figure 4.56c, an additional load path is provided to react the corner loads but at some mass penalty. Similar data for out-of-plane bending alternatives [11] are provided in Figure 4.57.

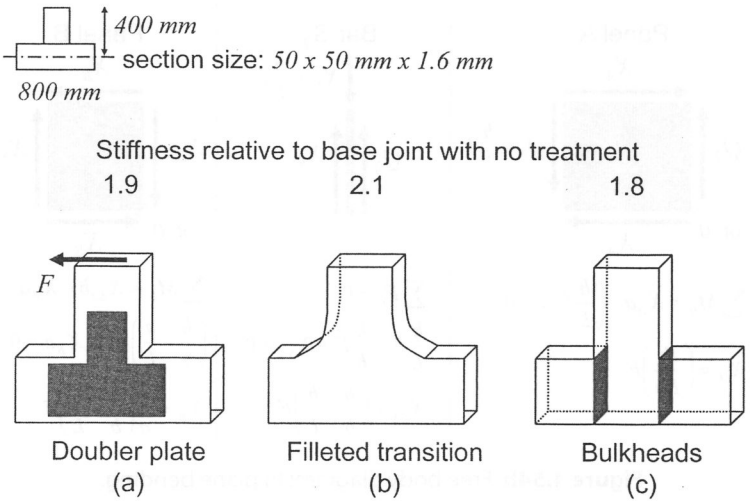

Figure 4.56 Increasing joint rigidity for in plane bending.

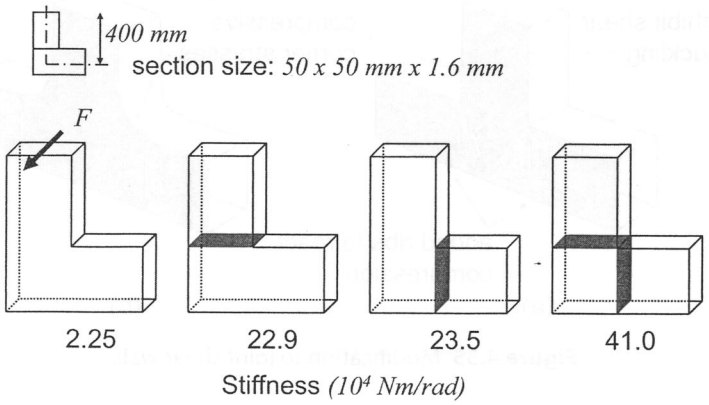

Figure 4.57 Effect of added bulkheads on out of plane joint rigidity.

4.5.1 Examples of body joint design

We have discussed joint design principles using an idealized set of rectangular beams. Now let us look at the application of these principles to more representative joints.

A-pillar-to-hinge-pillar joint

Figure 4.58a shows an A pillar and hinge pillar from a typical vehicle. The A-pillar surface is just behind the windshield edge, while the hinge pillar outer surface is considerably inboard due to positioning of the hinge attachment. This creates an undesirable lack of continuity for the shear surfaces of these two beams at the belt line. With careful coordination of exterior styling and door hinging, it is possible to achieve the alignment of the shear surface for both beams and a much stiffer joint, Figure 4.58b.

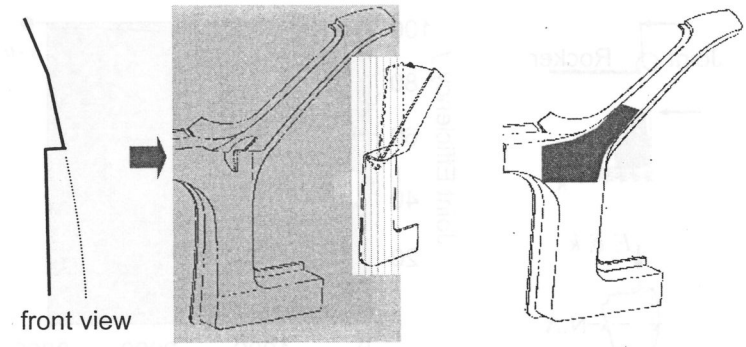

Figure 4.58 Hinge-pillar-to-A-pillar joint.

Hinge-pillar-to-rocker joint

Typical construction for the hinge-pillar-to-rocker joint is shown in Figure 4.59a. In many cases, there is an offset, *s*, between the inner shear plane of the rocker and the inner shear plane of the hinge pillar, Figure 4.59b. While we would ideally like these planes to be aligned with *s=0* for the stiffest joint, other constraints may prevent this from occurring. When *s>0*, the rocker section distorts under in-plane loading, as shown in Figure 4.59c. In this case, the rocker distortion behaves as a series of springs reacting the rotational motion of the hinge pillar, Figure 4.60a. (This is similar to the behavior of thin-walled sections under a point load which we looked at in Chapter 3.) The larger the offset, *s*, the more flexible is each slice of the rocker section. Figure 4.60b plots the joint efficiency vs. the rocker section stiffness for various offset dimensions. It can be seen that for relatively small offsets (*s>5 mm*), the joint efficiency is greatly reduced.

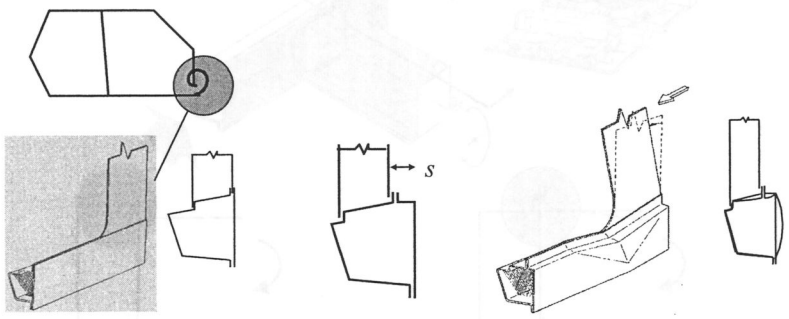

Figure 4.59 Lower-hinge-pillar-to-rocker joint.

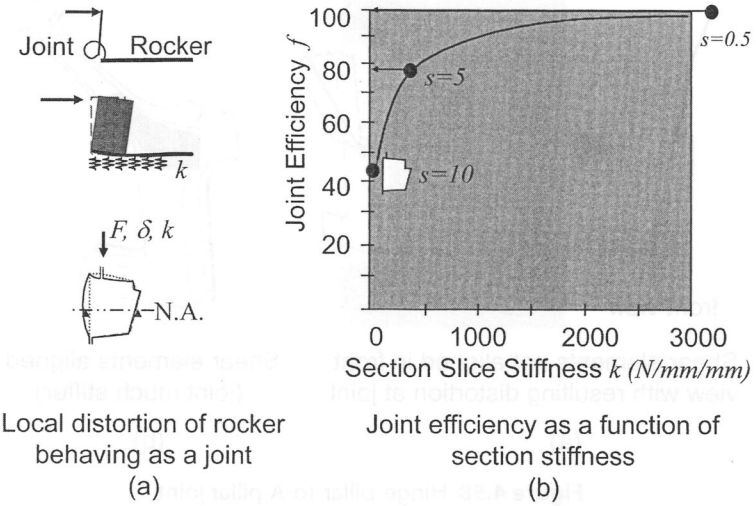

Figure 4.60 Joint efficiency of alternative rocker sections.

Floor-cross-member-to-rocker joint

The floor-cross-member-to-rocker joint shown in Figure 4.61 is loaded in out-of-plane bending. If the spot-weld flanges are perpendicular to the tensile and compressive loads in the top and bottom of the cross-member section, Figure 4.61a, the welds will be in peel and have considerable local distortion. By forming the weld flange as shown in Figure 4.61b, the loads are more nearly transferred in shear and a much stiffer joint results.

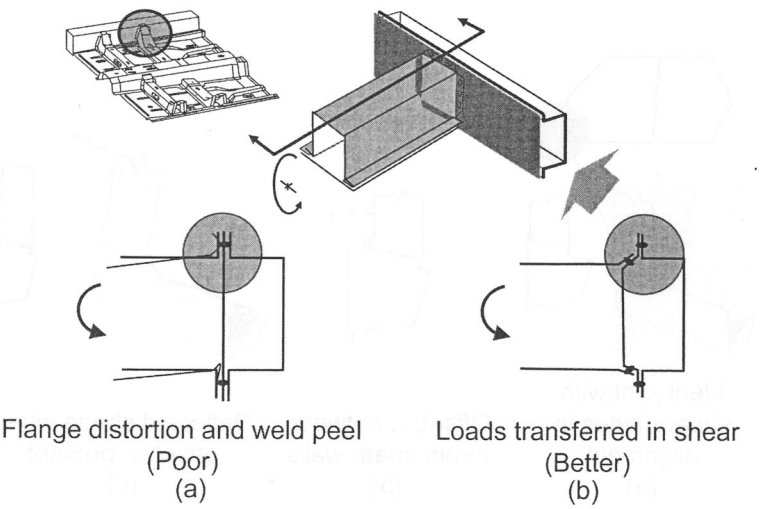

Figure 4.61 Seat-cross-member-to-rocker joint construction: Out-of-plane bending.

4.5.2 Joint behavior at abrupt geometric transitions

Thus far we have been considering the localized deformation at the physical attachment between two or more beams. Often we see a similar large localized defection within a single beam, which contains an abrupt geometric transition, Figure 4.62. Even though no physical joint is present, we can treat the transition area as a joint stiffness with a beam on either side. A notable example is a beam with two relatively straight portions and a central curved portion, Figure 4.63. If we look at in-plane bending for this beam, we would see that the curved portion has high localized angular deformation and acts as a flexible joint connecting the two straight portions of the beam. Isolating the curved portion and applying moments to either side gives rise to compressive stresses along the top surface and tensile stresses along the bottom surface, Figure 4.63a.

Now consider a side view of the curved section of the beam, Figure 4.63b. The compressive load, P, acts on the top surface of the section, and we can see that an upward force, w, is required to place the surface into static equilibrium, Figure 4.63b. The magnitude of this upward force is given by:

$$w = \frac{P}{R} \tag{4.12}$$

where:

w = Compressive force per unit length acting on web

P = Compressive force acting on the strip

R = Radius of curvature of the strip.

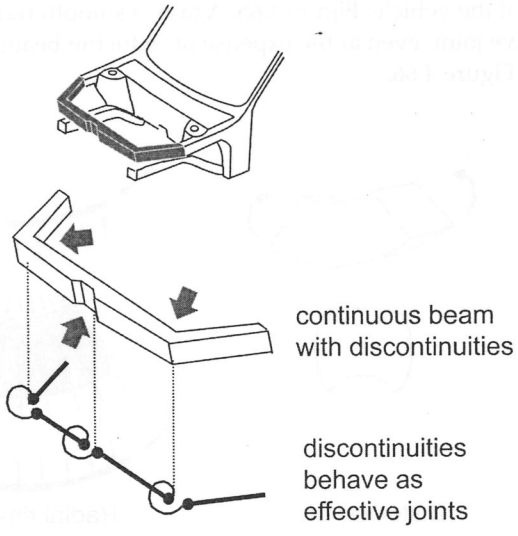

Figure 4.62 Changes in section causing local flexibility.

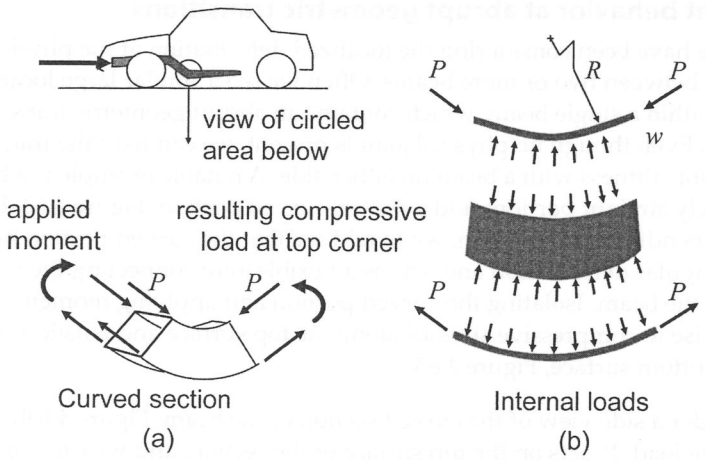

Figure 4.63 Effective joint for a curved beam.

This force, w, is a compressive force provided by the web of the beam pushing the upper and lower beam surfaces apart. Because the magnitude of this force is inversely proportional to the beam radius, beams with more abrupt curvature (smaller R) have a higher compressive force in the web. This compressive web force distorts the section, as shown in Figure 4.64a, and results in joint-like behavior. To improve this joint stiffness, the radius of curvature should be increased, or radial ribs included which react the compressive web loads, Figure 4.64b.

Often, the geometric transition is in a straight beam for the purpose of clearing some component of the vehicle, Figure 4.65. Again, a smooth transition will result in a stiffer effective joint, even at the expense of reducing beam section well before the component, Figure 4.66.

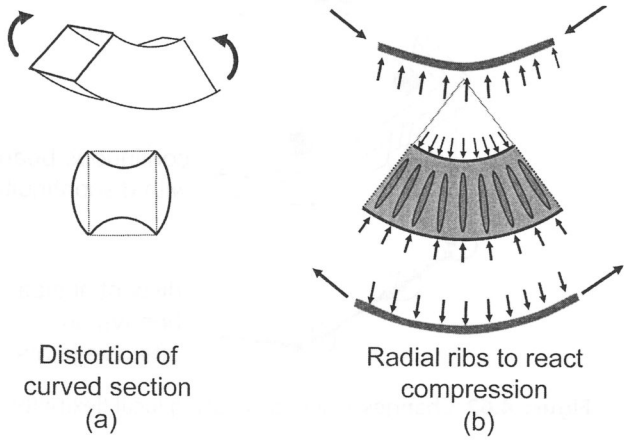

Figure 4.64 Stabilizing curved beam.

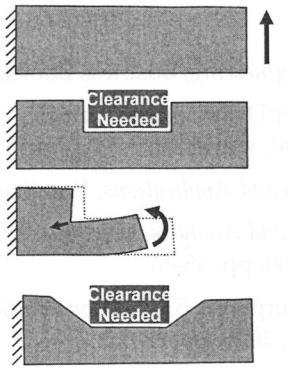

Figure 4.65 Section transition as a joint.

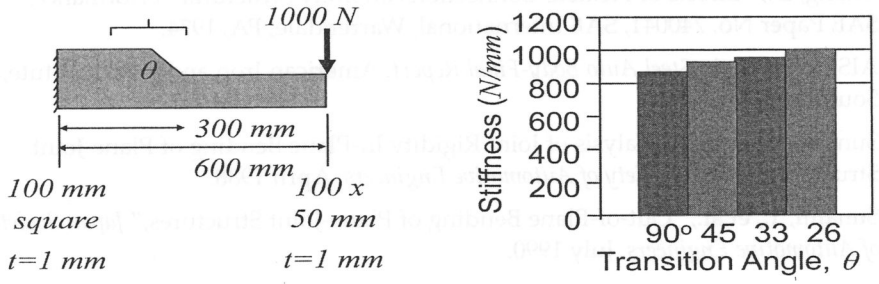

Figure 4.66 Smoothness of section transition.

4.5.3 Summary-Joint design

Two types of joint loading were defined—in-plane and out-of-plane, Figures 4.45 and 46. For in-plane loading, several design principles for stiff joint construction were presented. Shear walls of the connected beams should be aligned and flow smoothly from one beam to another, Figure 4.58. Even with the shear walls aligned in this way, however, the side wall at the beam intersection is relatively highly loaded in shear, and can be prone to shear buckling. Also the front and rear corners of the loaded beam place high compression stresses in the side wall, which is prone to compressive buckling, Figure 4.53. Careful placement of ribs or bulkheads can provide load paths for these conditions, Figures 4.55, 56, and 57. A severe geometric transition in a single beam can act as a flexible joint. To make this transition as stiff as possible, it should be gradual and smooth, Figures 4.64 and 66.

References

1. Pawlowski, J., *Vehicle Body Engineering*, Business Books, London, 1969, p. 124.
2. "Lincoln LS and the Parameter Development Vehicle," *Automotive Engineering International*, SAE International, Warrendale, PA, April, 1999, p. 32.
3. Thomson, W., *Vibration Theory and Applications*, Prentice-Hall, NJ, 1965, p. 275.
4. Fenton, J., *Vehicle Body Layout and Analysis*, Mechanical Engineering Publications, Ltd, London, 1980, pp. 55–57.
5. Brown, J.C., Robertson, A.J., Serpento, S.T., *Motor Vehicle Structures*, SAE International, Warrendale, PA, 2001, pp. 68–75.
6. Kikuchi, N. & Malen, D., Course notes for ME513 Fundamentals of Body Engineering, University of Michigan, Ann Arbor, MI, 2007.
7. Zienkiewicz, O. & Cheung, Y., *The Finite Element Method in Structural and Continuum Mechanics*, McGraw-Hill, NY, 1967.
8. Chang, D., "Effects of Flexible Connections on Body Structural Performance," SAE Paper No. 740041, SAE International, Warrendale, PA, 1974.
9. AISI, *Ultra Light Steel Auto Body-Final Report*, American Iron and Steel Institute, Southfield, MI, 1998.
10. Sunami, Y., et al., "Analysis of Joint Rigidity In-Plane Bending of Plane-Joint Structures," *Japan Society of Automotive Engineers*, April 1988.
11. Sunami, Y., et al., "Out-of-Plane Bending of Plane-Joint Structures," *Japan Society of Automotive Engineers*, July 1990.